Theory of Third-order Spectroscopic Methods to Extract Detailed Molecular Orientational Dynamics for Planar Surfaces and Other Uniaxial Systems

Jun Nishida, Michael D. Fayer*
Department of Chemistry, Stanford University, Stanford, CA 94305
*fayer@stanford.edu

Supplemental Material

A. Orthogonality of the Surface Frame Correlation Functions of the Spherical Harmonics

In Section II, Eqs. (II.17) and (II.18) played a central role in simplifying the response functions in terms of the correlation functions of spherical harmonics. Here, we will prove that Eqs. (II.17) and (II.18) are rigorously correct as long as the system is macroscopically symmetric in the surface plane. The correlation functions of interest, $\left\langle Y_2^{m'*}\left(\Omega_1\right)Y_2^m\left(\Omega_0\right)\right\rangle$, can be written as

$$\begin{aligned}
&\left\langle Y_2^{m'*}\left(\Omega_1\right)Y_2^m\left(\Omega_0\right)\right\rangle \\
&=\int_{\theta_1=0}^{\theta_1=\pi} d\theta_1 \int_{\phi_1=0}^{\phi_1=2\pi} d\phi_1 \int_{\theta_0=0}^{\theta_0=\pi} d\theta_0 \int_{\phi_0=0}^{\phi_0=2\pi} d\phi_0 \;\; Y_2^{m'*}(\theta_1,\phi_1)G(\theta_1,\phi_1,\theta_0,\phi_0,t)Y_2^m(\theta_0,\phi_0) \qquad \text{(B.1)}\\
&=\int_{\theta_1=0}^{\theta_1=\pi} d\theta_1 \int_{\theta_0=0}^{\theta_0=\pi} d\theta_0 \;\; (\theta\text{-dependent factor})\times\left[\int_{\phi_1=0}^{\phi_1=2\pi} d\phi_1 \int_{\phi_0=0}^{\phi_0=2\pi} d\phi_0 \;\; e^{-im'\phi_1}e^{im\phi_0}G(\theta_1,\phi_1,\theta_0,\phi_0,t)\right]
\end{aligned}$$

The spherical harmonics can always be factorized into a θ-dependent factor and a ϕ-dependent factor. We will focus on the ϕ integral in Eq.(B.1). When the ϕ integral is calculated, all the other variables in Green's function, θ_1, θ_2 and t, can be regarded as constants. Because the system is symmetric in-plane, i.e., in terms of azimuthal angle, Green's function can be written as

$$G(\theta_1,\phi_1,\theta_0,\phi_0,t)=g_{\theta_1,\theta_0,t}(\phi_1-\phi_0) \qquad \text{(B.2)}$$

where $g_{\theta_1,\theta_0,t}(x)$ satisfies

$$g_{\theta_1,\theta_0,t}(\phi+2\pi)=g_{\theta_1,\theta_0,t}(\phi) \qquad \text{(B.3)}$$

Eq. (B.2) says that the probability for a transition dipole moment to move from ϕ_1 to ϕ_2 (once θ_1, θ_2 and t are fixed) depends only on the difference between ϕ_1 and ϕ_2. Because movements by ϕ or $\phi + 2\pi$ are not distinguishable, Eq. (B.3) is valid. Then the ϕ-integral in Eq. (B.1) can be written further as

$$\begin{aligned}
&\int_{\phi_1=0}^{\phi_1=2\pi} d\phi_1 \int_{\phi_0=0}^{\phi_0=2\pi} d\phi_0 \; e^{-im'\phi_1} e^{im\phi_0} G(\theta_1, \phi_1, \theta_0, \phi_0, t) \\
&= \int_{\phi_1=0}^{\phi_1=2\pi} d\phi_1 \int_{\phi_0=0}^{\phi_0=2\pi} d\phi_0 \; e^{-im'\phi_1} e^{im\phi_0} g_{\theta_1,\theta_0,t}(\phi_1 - \phi_0) \\
&= \int_{\phi_1=0}^{\phi_1=2\pi} d\phi_1 \int_{\phi_0=0}^{\phi_0=2\pi} d\phi_0 \; e^{i(m-m')\phi_0} e^{-im'(\phi_1-\phi_0)} g_{\theta_1,\theta_0,t}(\phi_1 - \phi_0) \\
&\equiv \int_{\phi_1=0}^{\phi_1=2\pi} d\phi_1 \int_{\phi_0=0}^{\phi_0=2\pi} d\phi_0 \; e^{i(m-m')\phi_0} h_{\theta_1,\theta_0,t}(\phi_1 - \phi_0)
\end{aligned} \tag{B.4}$$

Note that $h_{\theta_1,\theta_0,t}(\phi) \equiv e^{-im'\phi} g_{\theta_1,\theta_0,t}(\phi)$ satisfies $h_{\theta_1,\theta_0,t}(\phi + 2\pi) = h_{\theta_1,\theta_0,t}(\phi)$ from Eq. (B.3). Thus $h_{\theta_1,\theta_0,t}(\phi_1 - \phi_0)$ can be expanded as a Fourier series in the form

$$h_{\theta_1,\theta_0,t}(\phi_1 - \phi_0) = \sum_{n=-\infty}^{\infty} c_n e^{-n(\phi_1-\phi_0)} \tag{B.5}$$

By substituting (B.5) into (B.4),

$$\begin{aligned}
&\int_{\phi_1=0}^{\phi_1=2\pi} d\phi_1 \int_{\phi_0=0}^{\phi_0=2\pi} d\phi_0 \; e^{i(m-m')\phi_0} h_{\theta_1,\theta_0,t}(\phi_1 - \phi_0) \\
&= \sum_{n=-\infty}^{\infty} c_n \int_{\phi_1=0}^{\phi_1=2\pi} d\phi_1 \int_{\phi_0=0}^{\phi_0=2\pi} d\phi_0 \; e^{i(m-m')\phi_0} \cdot e^{-in(\phi_1-\phi_0)} \\
&= \sum_{n=-\infty}^{\infty} c_n \int_{\phi_1=0}^{\phi_1=2\pi} d\phi_1 \; e^{-in\phi_1} \int_{\phi_0=0}^{\phi_0=2\pi} d\phi_0 \; e^{i[n-(m'-m)]\phi_0} \\
&= \sum_{n=-\infty}^{\infty} c_n \delta_{n,0} \delta_{n,m'-m} = c_0 \delta_{0,m'-m} \propto \delta_{0,m'-m}
\end{aligned} \tag{B.6}$$

As seen in Eq.(B.6), the ϕ integral in Eq. (B.1) is only non-zero when $m' = m$. Therefore, $\left\langle Y_2^{m'*}(\Omega_1) Y_2^m(\Omega_0) \right\rangle \propto \delta_{m',m}$, which is Eq. (II.17) . Eq. (II.18) can be proven in the exactly same manner by setting $m' = 0$ in the above.

B. Correlation Functions of the Spherical Harmonics in the Surface Frame for the Wobbling-in-a-Cone Model

1. Cone Normal to the Surface - Wang and Pecora

Wang and Pecora[1] solved the following differential equation for $W(\Omega, t)$,

$$\frac{\partial W(\Omega,t)}{\partial t} = D\nabla^2 W(\Omega,t) \tag{C.1}$$

with the boundary condition

$$\left.\frac{\partial W(\Omega,t)}{\partial \theta}\right|_{\theta=\theta_C} = 0 \tag{C.2}$$

$W(\Omega,t)$ is the probability a single transition dipole moment is pointing the direction of Ω. Based on their solution, they showed that in case the half-cone angle satisfies $\theta_C \le 60°$ the correlation functions we need here are almost perfectly approximated by

$$\left\langle Y_2^{0*}(t) Y_2^0(0) \right\rangle_{\theta_{\text{tilt}}=0^\circ} = \frac{5}{4\pi}\left(C_1^0 + C_2^0 e^{-\nu_2^0(\nu_2^0+1)Dt} \right) \tag{C.3}$$

$$\left\langle Y_2^{1*}(t) Y_2^1(0) \right\rangle_{\theta_{\text{tilt}}=0^\circ} = \frac{5}{8\pi} C_1^1 e^{-\nu_1^1(\nu_1^1+1)Dt} \tag{C.4}$$

$$\left\langle Y_2^{2*}(t) Y_2^2(0) \right\rangle_{\theta_{\text{tilt}}=0^\circ} = \frac{5}{8\pi} C_1^2 e^{-\nu_1^2(\nu_1^2+1)Dt} \tag{C.5}$$

where the C coefficients are the functions of cone angle θ_C:

$$C_1^0 = \frac{1}{4}\cos^2\theta_C \left(1+\cos\theta_C\right)^2 \tag{C.6}$$

$$C_2^0 = \frac{1}{20}\left(4 - \cos\theta_C - 6\cos^2\theta_C - \cos^3\theta_C + 4\cos^4\theta_C\right) \quad \text{(C.7)}$$

$$C_1^1 = \frac{1}{5}\left\{2 + 2\cos\theta_C(1+\cos\theta_C) - 3\cos^3\theta_C(1+\cos\theta_C)\right\} \quad \text{(C.8)}$$

$$C_1^2 = \frac{1}{20}\left\{8 - 7\cos\theta_C(1+\cos\theta_C) + 3\cos^3\theta_C(1+\cos\theta_C)\right\} \quad \text{(C.9)}$$

ν_2^0, ν_1^1 and ν_1^2 also depend on θ_C. There is no analytical form for these parameters, but the following approximate formulas based on numerical calculations are applicable for $\theta_C \le 170°$ [2,3]:

$$\nu_2^0 \approx \nu_1^2 \approx 10^{0.496}\theta_C^{-1.122} \quad \text{(C.10)}$$

$$\nu_1^1 \approx 10^{0.237}\theta_C^{-1.122} \quad \text{(C.11)}$$

Also, the time-average of Y_2^0 is given by

$$\left\langle Y_2^0 \right\rangle_{\theta_{\text{tilt}}=0°} = \sqrt{\frac{5}{16\pi}}\cos\theta_C\left(1+\cos\theta_C\right) \quad \text{(C.12)}$$

Eqs.(C.3), (C.5) and (C.12) are necessary to calculate the response functions for a transition dipole wobbling in a normal cone.

2. Tilted Cone

A tilted cone is illustrated in Figure S1. Here we derive the correlation functions of the spherical harmonics for a transition dipole in the titled cone in the surface frame (*S*); these are used in Eqs. (II.21), (II.22) and (II.31) to calculate the response functions. In the conical frame (*C*), shown as (X_C, Y_C, Z_C) in Figure S1, the correlation functions are clearly given by

$$\left\langle Y_2^{m*}(t)Y_2^m(0)\right\rangle_C = \left\langle Y_2^{m*}(t)Y_2^m(0)\right\rangle_{\theta_{\text{tilt}}=0°}. \quad \text{(C.13)}$$

Once the spherical harmonics in surface frame can be expressed in terms of those in

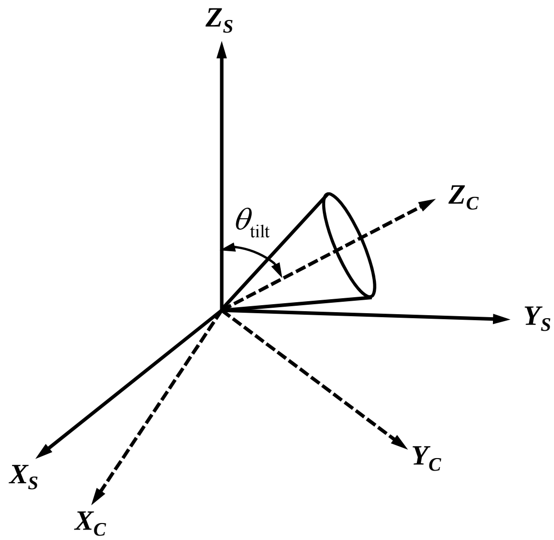

Figure S1. The definition of the Conical Frame (X_C, Y_C, Z_C) with respect to the Surface Frame (X_S, Y_S, Z_S). The transition dipole is wobbling in a normal cone in the Conical Frame.

conical frame, then the correlation functions can be calculated using Eq. (C.13). Addition theorem for the spherical harmonics can be used for this purpose:[4]

$$Y_2^m(\Omega_S) = \sum_{m'} D^2_{m'm}(\phi_{SC}, \theta_{SC}, \chi_{SC}) Y_2^{m'}(\Omega_C), \tag{C.14}$$

where $D^2_{m'm}(\phi_{SC}, \theta_{SC}, \chi_{SC})$ is the second order Wigner *D* matrix

$$D^2_{m'm}(\phi_{SC}, \theta_{SC}, \chi_{SC}) = e^{-i\phi_{SC}m'} d^2_{m'm}(\theta_{SC}) e^{-i\chi_{SC}m} \tag{C.15}$$

The Wigner small *d* matrix $d^2_{m'm}(\theta)$ can be found in literature.[4] $(\phi_{SC}, \theta_{SC}, \chi_{SC})$ are the Euler angles that transfer the conical frame (X_C, Y_C, Z_C) into the surface frame (X_S, Y_S, Z_S). Based on Figure S1, the Euler angles for this procedure is $\phi_{SC} = 0$, $\theta_{SC} = -\theta_{\text{tilt}}$. χ_{SC} depends on the azimuthal directions of the primary axis of the cone in the surface frame. Thus, Eq. (C.14) can be written as

$$Y_2^m(\Omega_S) = e^{-i\chi_{SC}m} \sum_{m'} d^2_{m'm}(-\theta_{\text{tilt}}) Y_2^{m'}(\Omega_C) \tag{C.16}$$

Using Eq. (C.16), the correlation functions of interest are generally expressed as

$$\begin{aligned}\left\langle Y_2^{m'*}(t)Y_2^m(0)\right\rangle_S^{\chi_{SC}} &= e^{-i\chi_{SC}(m-m')}\sum_{k,k'} d_{k'm'}^2(-\theta_{\text{tilt}})d_{km}^2(-\theta_{\text{tilt}})\left\langle Y_2^{k'*}(t)Y_2^k(0)\right\rangle_C \\ &= e^{-i\chi_{SC}(m-m')}\sum_{k} d_{km'}^2(-\theta_{\text{tilt}})d_{km}^2(-\theta_{\text{tilt}})\left\langle Y_2^{k*}(t)Y_2^k(0)\right\rangle_C\end{aligned} \tag{C.17}$$

Here, the orthogonality of the spherical harmonics in the conical frame is used. Eq. (C.17) is the correlation function for a cone tilted to a specific azimuthal direction specified by χ_{SC}. Because of the in-plane symmetry of the surface, the azimuthal direction of the primary axis of the cones should be randomly oriented on the surface. Then, the actual ensemble average correlation functions in the surface frame can be calculated by

$$\left\langle Y_2^{m'*}(t)Y_2^m(0)\right\rangle_S = \frac{1}{2\pi}\int_0^{2\pi} d\chi_{SC}\left\langle Y_2^{m'*}(t)Y_2^m(0)\right\rangle_S^{\chi_{SC}} \tag{C.18}$$

It is clear from Eqs. (C.17) and (C.18) that $\left\langle Y_2^{m'*}(t)Y_2^m(0)\right\rangle_S \propto \delta_{m'm}$, which we proved for the general case in Section A above. From Eqs. (C.17) and (C.18),

$$\begin{aligned}\left\langle Y_2^{0*}(t)Y_2^0(0)\right\rangle_S &= \frac{1}{4}\left(3\cos^2\theta_{\text{tilt}}-1\right)^2\left\langle Y_2^{0*}Y_2^0\right\rangle_C + 3\sin^2\theta_{\text{tilt}}\cos^2\theta_{\text{tilt}}\left\langle Y_2^{1*}Y_2^1\right\rangle_C \\ &\quad + \frac{3}{4}\sin^4\theta_{\text{tilt}}\left\langle Y_2^{2*}Y_2^2\right\rangle_C\end{aligned} \tag{C.19}$$

$$\begin{aligned}\left\langle Y_2^{1*}(t)Y_2^1(0)\right\rangle_S &= \frac{3}{2}\sin^2\theta_{\text{tilt}}\cos^2\theta_{\text{tilt}}\left\langle Y_2^{0*}Y_2^0\right\rangle_C + \frac{1}{4}\left(2+\cos 2\theta_{\text{tilt}}+\cos 4\theta_{\text{tilt}}\right)\left\langle Y_2^{1*}Y_2^1\right\rangle_C \\ &\quad + \frac{1}{2}\sin^2\theta_{\text{tilt}}\left(\cos^2\theta_{\text{tilt}}+1\right)\left\langle Y_2^{2*}Y_2^2\right\rangle_C\end{aligned} \tag{C.20}$$

$$\begin{aligned}\left\langle Y_2^{2*}(t)Y_2^2(0)\right\rangle_S &= \frac{3}{8}\sin^4\theta_{\text{tilt}}\left\langle Y_2^{0*}Y_2^0\right\rangle_C + \frac{1}{2}\sin^2\theta_{\text{tilt}}\left(\cos^2\theta_{\text{tilt}}+1\right)\left\langle Y_2^{1*}Y_2^1\right\rangle_C \\ &\quad + \left\{\sin^8\frac{\theta_{\text{tilt}}}{2}+\cos^8\frac{\theta_{\text{tilt}}}{2}\right\}\left\langle Y_2^{2*}Y_2^2\right\rangle_C\end{aligned} \tag{C.21}$$

$$\left\langle Y_2^0(t)\right\rangle_S = \frac{3\cos^2\theta_{\text{tilt}}-1}{2}\cdot\left\langle Y_2^0\right\rangle_C \tag{C.22}$$

Using (C.13), together with (C.2)-(C.5) and (C.12), (C.19)-(C.22) can be written more explicitly as

$$\left\langle Y_2^{0*}(t)Y_2^0(0)\right\rangle_{\theta_{\text{tilt}}} = \frac{5}{16\pi}\left(3\cos^2\theta_{\text{tilt}}-1\right)^2\left[C_1^0+C_2^0 e^{-\nu_2^0(\nu_2^0+1)Dt}\right]+\frac{15}{8\pi}\sin^2\theta_{\text{tilt}}\cos^2\theta_{\text{tilt}}C_1^1 e^{-\nu_1^1(\nu_1^1+1)Dt} + \frac{15}{32\pi}\sin^4\theta_{\text{tilt}}C_1^2 e^{-\nu_1^2(\nu_1^2+1)Dt} \tag{C.23}$$

$$\left\langle Y_2^{1*}(t)Y_2^1(0)\right\rangle_{\theta_{\text{tilt}}} = \frac{15}{8\pi}\sin^2\theta_{\text{tilt}}\cos^2\theta_{\text{tilt}}\left[C_1^0+C_2^0 e^{-\nu_2^0(\nu_2^0+1)Dt}\right]+\frac{5}{32\pi}\left(2+\cos 2\theta_{\text{tilt}}+\cos 4\theta_{\text{tilt}}\right)C_1^1 e^{-\nu_1^1(\nu_1^1+1)Dt} + \frac{5}{16\pi}\sin^2\theta_{\text{tilt}}\left(\cos^2\theta_{\text{tilt}}+1\right)C_1^2 e^{-\nu_1^2(\nu_1^2+1)Dt} \tag{C.24}$$

$$\left\langle Y_2^{2*}(t)Y_2^2(0)\right\rangle_{\theta_{\text{tilt}}} = \frac{15}{32\pi}\sin^4\theta_{\text{tilt}}\left[C_1^0+C_2^0 e^{-\nu_2^0(\nu_2^0+1)Dt}\right]+\frac{5}{16\pi}\sin^2\theta_{\text{tilt}}\left(1+\cos^2\theta_{\text{tilt}}\right)C_1^1 e^{-\nu_1^1(\nu_1^1+1)Dt} + \frac{5}{8\pi}\left\{\sin^8\frac{\theta_{\text{tilt}}}{2}+\cos^8\frac{\theta_{\text{tilt}}}{2}\right\}C_1^2 e^{-\nu_1^2(\nu_1^2+1)Dt} \tag{C.25}$$

$$\left\langle Y_2^0(t)\right\rangle_{\theta_{\text{tilt}}} = \sqrt{\frac{5}{16\pi}}\frac{3\cos^2\theta_{\text{tilt}}-1}{2}\cos\theta_C\left(1+\cos\theta_C\right) \tag{C.26}$$

It should be noted that under the approximations given in Eqs. (C.10) and (C.11), the time-dependent correlation functions decay as bi-exponentials, which leads to bi-exponential decays in the orientational response functions.

From (C.23) and (C.25), the correlation functions at infinitely long time are given by

$$\left\langle Y_2^{0*}(\infty)Y_2^0(0)\right\rangle_{\theta_{\text{tilt}}} = \frac{5}{16\pi}\left(3\cos^2\theta_{\text{tilt}}-1\right)^2 C_1^0 \tag{C.27}$$

$$\left\langle Y_2^{2*}(\infty)Y_2^2(0)\right\rangle_{\theta_{\text{tilt}}} = \frac{15}{32\pi}\sin^4\theta_{\text{tilt}}C_1^0, \tag{C.28}$$

which are dependent both on the cone angle θ_C and the tilt angle θ_{tilt}.

3. Consideration of the Roughness of the Surface

The addition theorem of spherical harmonics can be also used to take local roughness of the surface into account. By surface roughness, we mean that local macroscopic regions of the surface are tilted at various angles relative to an ideal perfect plane. Variations in the thickness of a monolayer do not matter. In case the surface is rough, the frame in which the correlation functions are calculated is tilted from the actual surface frame by a certain angle. This is exactly the situation that occurs in the transformation from conical frame to surface frame discussed above. Thus the same strategy can be employed here. The spherical harmonics correlation functions for rough surface can be calculated by

$$\left\langle Y_2^{m*}(t)Y_2^m(0)\right\rangle_{\text{rough,S}} = \int d\theta\; G(\theta)\left[\sum_k \left\{d_{km}^2(-\theta)\right\}^2 \left\langle Y_2^{k*}(t)Y_2^k(0)\right\rangle_{\text{flat,S}}\right] \qquad \text{(C.29)}$$

where $\left\langle Y_2^{k*}(t)Y_2^k(0)\right\rangle_{\text{flat,S}}$ is the correlation function calculated assuming the surface supporting the monolayer is flat and $\left\langle Y_2^{m*}(t)Y_2^m(0)\right\rangle_{\text{rough,S}}$ is the correlation function for the rough surface, which should be used in the calculation of response functions. The quantity in […] corresponds to the correlation function for monolayer on the surface which is tilted exactly by angle θ from the ideal surface normal. $G(\theta)$ is the weighing factor which depends on the nature of the roughness of the surface. Again, the in-plane symmetry of the surface is assumed in the derivation of Eq. (B.29). Using Eq. (B.29), once the local roughness of the surface is characterized, e. g., by atomic force microscopy, to provide $G(\theta)$, the correlation functions necessary to simulate response functions can be readily obtained from the correlation functions calculated with the assumption that the surface is ideally flat. It is important to note that for a reasonably high quality surface if the angular deviations of the surface relative to a perfect plane are only a few degrees, the roughness will introduce negligible error compared to error bars that are likely to arise in real experimental measurements.

C. Modifications of the Response Functions for Beams with Significant Crossing Angles and Fluorescence with a Substantial Collection Cone

In Section V, the orientational response functions were presented for the different experiments: pump-probe, heterodyne detected transient grating (HDTG) with all of the beams in a plane, HDTG with BOXCARS geometry, and the fluorescence geometry. In Figures 9 and 10, each polarization is relative to the beam propagation direction (*B* – beam frame), with Z_B along the beam propagation direction, and X_B and Y_B are perpendicular to Z_B. X_B is in the X_LZ_L plane, while Y_B is in the Y_LZ_L plane. All of the response functions polarization subscripts are in the beam frame in this and following sections, but for brevity, the subscripts *B* have been omitted. Prior to Section V, all of the beams are collinear, so the polarizations are the same in the beam frame and the lab frame.

As discussed in the text, for the pump-probe geometry in Figure 9A, no modification is necessary to the formulas given in Eqs. (II.21), (II.22) and (II.31), because the X_B and Y_B polarizations of the beams coincide with X_L and Y_L axes in the lab frame. The derivations of the formulas for the other geometries are provided below.

For BOXCARS and fluorescence geometries, the horizontal crossing angle Φ or the fluorescence collection cone angle Θ must be set sufficiently small so that the amplitude difference between $R_{XXXX}^{\chi=0^\circ}$ and $R_{XXXX}^{\chi\neq0^\circ}$ is negligible, as mentioned in Section V. For BOXCARS geometry, small Φ is also important to avoid a significant contribution of $\langle Y_2^{1*}Y_2^1\rangle$ in $R_{XXXX}^{\chi=0^\circ}$. The maximum acceptable Θ and Φ are also discussed.

1. Transient Grating Geometry – Beams in a Plane

In the configuration shown in Figure 9B, the X_B polarizations of all the beams coincide exactly with the X_L direction in the lab frame, whereas the Y_B polarizations of B1 and B2 are not parallel to the Y_L direction in the lab frame; the Y_B polarizations for B1 and B2 can be represented by the linear combination of the polarizations along Y_L direction and Z_L directions.

$$\hat{\varepsilon}_{Y_{B1}} = \cos\Phi \cdot \hat{\varepsilon}_{Y_L} - \sin\Phi \cdot \hat{\varepsilon}_{Z_L} \tag{D.1}$$

$$\hat{\varepsilon}_{Y_{B2}} = \cos\Phi \cdot \hat{\varepsilon}_{Y_L} + \sin\Phi \cdot \hat{\varepsilon}_{Z_L} \tag{D.2}$$

In case $\chi = 0°$, as shown in Eqs. (II.6) and (II.7), the E-fields in lab frame (L) and surface frame (S) coincide with each other. Thus, for example, the response function $R_{XXYY}^{\chi=0^\circ}$ can be calculated by

$$\begin{aligned} R_{XXYY}^{\chi=0^\circ}(t) &= \int d\Omega_1 \int d\Omega_0 (\hat{\mu}_1 \hat{\varepsilon}_{X_{B,TG}})(\hat{\mu}_1 \hat{\varepsilon}_{X_{B3}}) G(\Omega_1, t | \Omega_0)(\hat{\mu}_0 \hat{\varepsilon}_{Y_{B2}})(\hat{\mu}_0 \hat{\varepsilon}_{Y_{B1}}) \\ &= \int d\Omega_1 \int d\Omega_0 (\hat{\mu}_1 \hat{\varepsilon}_{X_S})^2 G(\Omega_1, t | \Omega_0) \\ &\qquad (\cos\Phi \cdot \hat{\mu}_0 \hat{\varepsilon}_{Y_S} + \sin\Phi \cdot \hat{\mu}_0 \hat{\varepsilon}_{Z_S})(\cos\Phi \cdot \hat{\mu}_0 \hat{\varepsilon}_{Y_S} - \sin\Phi \cdot \hat{\mu}_0 \hat{\varepsilon}_{Z_S}) \end{aligned} \tag{D.3}$$

To make the calculation clear, the following integral is defined:

$$\left\langle \delta\gamma\beta\alpha \right\rangle_S \equiv \int d\Omega_1 \int d\Omega_0 (\hat{\mu}_1 \hat{\varepsilon}_{\delta S})(\hat{\mu}_1 \hat{\varepsilon}_{\gamma S}) G(\Omega_1, t | \Omega_0)(\hat{\mu}_0 \hat{\varepsilon}_{\beta S})(\hat{\mu}_0 \hat{\varepsilon}_{\alpha S}) \tag{D.4}$$

The spherical harmonics representations for $\left\langle \delta\gamma\beta\alpha \right\rangle_S$ (surface frame) are listed in Table S.1. Note that the integral such as $\left\langle XXYZ \right\rangle_S$ is zero. Eq. (D.3) can then be written as

$$R_{XXYY}^{\chi=0^\circ}(t) = \cos^2\Phi \left\langle XXYY \right\rangle_S - \sin^2\Phi \left\langle XXZZ \right\rangle_S \tag{D.5}$$

Using Table S.1, Eq. (D.5) can be rewritten in terms of spherical harmonics as

$$\begin{aligned} R_{XXYY}^{\chi=0^\circ}(t) &= \frac{1}{9}\cos 2\Phi - \frac{2}{9}\sqrt{\frac{\pi}{5}}\left(2\cos^2\Phi + \sin^2\Phi\right)\left\langle Y_2^0 \right\rangle \\ &\quad + \frac{4}{45}\pi\left(\cos^2\Phi + 2\sin^2\Phi\right)\left\langle Y_2^{0*} Y_2^0 \right\rangle - \frac{4}{15}\pi\cos^2\Phi\left\langle Y_2^{2*} Y_2^2 \right\rangle \end{aligned} \tag{D.6}$$

The same procedure can be followed to calculate $R_{XXXX}^{\chi=0^\circ}$, R_{XXXX}^{χ} and R_{XXYY}^{χ}. Note that for $\chi \neq 0$, in addition to the conversion from the beam frame to lab frame (Eqs. (D.1) and(D.2)), the lab frame must be further converted to surface frame using Eqs. (II.8) and (II.9). The results are shown in Eqs. (V.1)-(V.3) in the main text.

2. BOXCARS Geometry

To calculate the response functions for both $\chi = 0$ and $\chi \neq 0$ (shown in Figure 10A), again the polarization of each beam (*B* – beam frame) must first be converted to polarizations in the lab frame taking into consideration the crossing angle, and then into the surface frame taking into account χ. Then, the surface frame unit vectors obtained from the lab frame vectors are used to calculate the response functions as in Section C.1, Eq.(D.3).

The conversion formulas from *B* to *L* are given in the following Eqs. (C.7)-(C.12) where $\hat{\varepsilon}_{X_{Bi}}$ and $\hat{\varepsilon}_{Y_{Bi}}$ corresponds to *X*- and *Y*-polarization of the i^{th} beam in the beam frame (see Figure 10A), and $\hat{\varepsilon}_{X_{B,TG}}$ is the detected polarization of the emitted transient grating signal in the beam frame:

$$\hat{\varepsilon}_{X_{B1}} = \cos\Phi \cdot \hat{\varepsilon}_{X_L} + \sin\Phi \cdot \hat{\varepsilon}_{Z_L} \qquad \text{(D.7)}$$

$$\hat{\varepsilon}_{Y_{B1}} = \hat{\varepsilon}_{Y_L} \qquad \text{(D.8)}$$

$$\hat{\varepsilon}_{X_{B2}} = \hat{\varepsilon}_{X_L} \qquad \text{(D.9)}$$

$$\hat{\varepsilon}_{Y_{B2}} = \cos\Phi \cdot \hat{\varepsilon}_{Y_L} + \sin\Phi \cdot \hat{\varepsilon}_{Z_L} \qquad \text{(D.10)}$$

$$\hat{\varepsilon}_{X_{B3}} = \hat{\varepsilon}_{X_L} \qquad \text{(D.11)}$$

$$\hat{\varepsilon}_{X_{B,\mathrm{TG}}} = \cos\Phi \cdot \hat{\varepsilon}_{X_L} - \sin\Phi \cdot \hat{\varepsilon}_{Z_L}\,. \qquad \text{(D.12)}$$

The polarizations in the lab frame (L) have to be again converted to surface frame (S) especially when sample's tilt angle χ is not zero. In addition to Eqs. (II.8) and (II.9), the following conversion formula to convert $\hat{\varepsilon}_{Z_L}$ to surface frame is necessary:

$$\hat{\varepsilon}_{Z_L} = \cos\chi \cdot \hat{\varepsilon}_{Z_S} - \sin\chi \cdot \hat{\varepsilon}_{Y_S} \tag{D.13}$$

For example, Eq. (D.7) can be converted to surface frame in the form of

$$\hat{\varepsilon}_{X_{B1}} = \cos\Phi \cdot \hat{\varepsilon}_{X_S} - \sin\Phi \sin\chi \cdot \hat{\varepsilon}_{Y_S} + \sin\Phi \cos\chi \cdot \hat{\varepsilon}_{Z_S} \tag{D.14}$$

Other input polarizations can be converted to the surface frame as well. Then, for example, the *XXXX* signal for a tilt angle χ can be written as

$$\begin{aligned} R_{XXXX}^{\chi}(t) &= \int d\Omega_1 \int d\Omega_0 (\hat{\mu}_1 \hat{\varepsilon}_{X_{B,TG}})(\hat{\mu}_1 \hat{\varepsilon}_{X_{B3}}) G(\Omega_1, t | \Omega_0)(\hat{\mu}_0 \hat{\varepsilon}_{X_{B2}})(\hat{\mu}_0 \hat{\varepsilon}_{X_{B1}}) \\ &= \int d\Omega_1 \int d\Omega_0 \left(\cos\Phi \cdot \hat{\mu}_0 \hat{\varepsilon}_{X_L} - \sin\Phi \cdot \hat{\mu}_0 \hat{\varepsilon}_{Z_L}\right)(\hat{\mu}_1 \hat{\varepsilon}_{X_L}) G(\Omega_1, t | \Omega_0) \\ &\qquad (\hat{\mu}_0 \hat{\varepsilon}_{X_L})\left(\cos\Phi \cdot \hat{\mu}_0 \hat{\varepsilon}_{X_L} + \sin\Phi \cdot \hat{\mu}_0 \hat{\varepsilon}_{Z_L}\right) \\ &= \int d\Omega_1 \int d\Omega_0 \left(\cos\Phi \cdot \hat{\varepsilon}_{X_S} + \sin\Phi \sin\chi \cdot \hat{\varepsilon}_{Y_S} - \sin\Phi \cos\chi \cdot \hat{\varepsilon}_{Z_S}\right)(\hat{\mu}_1 \hat{\varepsilon}_{X_S}) G(\Omega_1, t | \Omega_0) \\ &\qquad (\hat{\mu}_0 \hat{\varepsilon}_{X_S})\left(\cos\Phi \cdot \hat{\varepsilon}_{X_S} - \sin\Phi \sin\chi \cdot \hat{\mu}_0 \hat{\varepsilon}_{Y_S} + \sin\Phi \cos\chi \cdot \hat{\mu}_0 \hat{\varepsilon}_{Z_S}\right) \end{aligned} \tag{D.15}$$

The orientational response functions can be written in the spherical harmonics representation using Table S.1. The results are shown in the main text, but repeated below for convenience:

$$\begin{aligned} R_{XXXX}^{\chi=0^\circ} &= \cos^2\Phi \langle XXXX \rangle_S - \sin^2\Phi \langle ZXXZ \rangle_S \\ &= \cos^2\Phi \left[\frac{1}{9} - \frac{4}{9}\sqrt{\frac{\pi}{5}} \langle Y_2^0 \rangle + \frac{4}{45}\pi \langle Y_2^{0*} Y_2^0 \rangle + \frac{4}{15}\pi \langle Y_2^{2*} Y_2^2 \rangle \right] \\ &\qquad - \sin^2\Phi \left\{ \frac{4}{15}\pi \langle Y_2^{1*} Y_2^1 \rangle \right\} \end{aligned} \tag{D.16}$$

$$\begin{aligned} R_{XXYY}^{\chi=0^\circ} &= \cos^2\Phi \langle XXYY \rangle_S \\ &= \cos^2\Phi \left[\frac{1}{9} - \frac{4}{9}\sqrt{\frac{\pi}{5}} \langle Y_2^0 \rangle + \frac{4}{45}\pi \langle Y_2^{0*} Y_2^0 \rangle - \frac{4}{15}\pi \langle Y_2^{2*} Y_2^2 \rangle \right] \end{aligned} \tag{D.17}$$

$$
\begin{aligned}
R_{XXXX}^{\chi} &= \cos^2\Phi\left\langle XXXX\right\rangle_S - \sin^2\Phi\cos^2\chi\left\langle ZXXZ\right\rangle_S - \sin^2\Phi\sin^2\chi\left\langle YXXY\right\rangle_S \\
&= \cos^2\Phi\left[\frac{1}{9}-\frac{4}{9}\sqrt{\frac{\pi}{5}}\left\langle Y_2^0\right\rangle+\frac{4}{45}\pi\left\langle Y_2^{0*}Y_2^0\right\rangle+\frac{4}{15}\pi\left\langle Y_2^{2*}Y_2^2\right\rangle\right] \\
&\quad -\sin^2\Phi\cos^2\chi\left\{\frac{4}{15}\pi\left\langle Y_2^{1*}Y_2^1\right\rangle\right\}-\sin^2\Phi\sin^2\chi\left\{\frac{4}{15}\pi\left\langle Y_2^{2*}Y_2^2\right\rangle\right\}
\end{aligned}
\tag{D.18}
$$

$$
\begin{aligned}
R_{XXYY}^{\chi} &= \cos\Phi\cos(\chi+\Phi)\cos\chi\left\langle XXYY\right\rangle_S + \cos\Phi\sin(\chi+\Phi)\sin\chi\left\langle XXZZ\right\rangle_S \\
&= \frac{1}{9}\cos^2\Phi-\frac{2}{9}\sqrt{\frac{\pi}{5}}\left\{2\cos\Phi\cos\left(\chi+\Phi\right)\cos\chi-\cos\Phi\sin\left(\chi+\Phi\right)\sin\chi\right\}\left\langle Y_2^0\right\rangle \\
&\quad +\frac{4\pi}{45}\left\{\cos\Phi\cos\left(\chi+\Phi\right)\cos\chi-2\cos\Phi\sin\left(\chi+\Phi\right)\sin\chi\right\}\left\langle Y_2^{0*}Y_2^0\right\rangle \\
&\quad -\frac{4\pi}{15}\cos\Phi\cos\left(\chi+\Phi\right)\cos\chi\left\langle Y_2^{2*}Y_2^2\right\rangle
\end{aligned}
\tag{D.19}
$$

Considering Eqs. (D.16)-(D.19), there are two issues in regard to the orientational correlation functions that need to be addressed. First, $R_{XXXX}^{\chi=0^\circ}$ contains $\left\langle Y_2^{1*}Y_2^1\right\rangle$, which does not show up for collinear beams (zero crossing angle) or for the geometries described above. As a result, the orientational correlation functions cannot be rigorously extracted from three measurements ($R_{XXXX}^{\chi=0^\circ}$, $R_{XXYY}^{\chi=0^\circ}$ and R_{XXYY}^{χ}), because there are four unknown parameters, $\left\langle Y_2^{0*}Y_2^0\right\rangle$, $\left\langle Y_2^{1*}Y_2^1\right\rangle$, $\left\langle Y_2^{2*}Y_2^2\right\rangle$ and $P(t)$. Another issue is that $R_{XXXX}^{\chi=0^\circ}$ is no longer equal to R_{XXXX}^{χ} as can be seen by comparing Eqs. (D.16) and (D.18). Thus the difference in the configuration factor (Eq. (II.39)) cannot be accounted for rigorously by examining the intensity ratio of the *XXXX* signals for $\chi = 0°$ and $\chi \neq 0°$. To account for these two effects and extract orientational correlation functions with the same scheme used for collinear beams, the horizontal crossing angle Φ should be set small enough (the small-crossing-angle limit) so that

$$
\begin{aligned}
R_{XXXX}^{\chi=0^\circ} &\approx R_{XXXX,\text{approx}}^{\chi=0^\circ} \\
&= \cos^2\Phi \left\langle XXXX \right\rangle_S \\
&= \cos^2\Phi \left[\frac{1}{9} - \frac{4}{9}\sqrt{\frac{\pi}{5}} \left\langle Y_2^0 \right\rangle + \frac{4}{45}\pi \left\langle Y_2^{0*} Y_2^0 \right\rangle + \frac{4}{15}\pi \left\langle Y_2^{2*} Y_2^2 \right\rangle \right]
\end{aligned}
\tag{D.20}
$$

and

$$
R_{XXXX}^{\chi=0^\circ} \approx R_{XXXX}^{\chi} . \tag{D.21}
$$

When the approximations given by Eqs. (D.20) and (D.21) are valid, the ratio of the configuration factor in Eq. (II.39) can be found by comparing the ratio of $R_{XXXX}^{\chi=0^\circ}$ and R_{XXXX}^{χ}, and then $\left\langle Y_2^{0*} Y_2^0 \right\rangle$, $\left\langle Y_2^{2*} Y_2^2 \right\rangle$ and $P(t)$ are obtained by solving Eqs.(D.20), (D.17) and (D.19), each multiplied by $\times P(t)$.

To be in the small angle limit, the acceptable crossing angle must be determined. As can be seen by examining Eqs. (D.16) and (D.20), the errors introduced by the approximations depend on each time averaged and time dependent parameters. Therefore, the properties of the monolayer of interest determine how large the crossing angle can be and still avoid significant error. The key to addressing these issue is the fact that Eq. (D.20) is essentially the approximation that neglects the contribution of $\left\langle ZXXZ \right\rangle_S$ in favor of $\left\langle XXXX \right\rangle_S$. The average polar angle of the transition dipoles in the surface frame, $\left\langle \theta_S \right\rangle$, is closely related to the error introduced by the approximation. If $\left\langle \theta_S \right\rangle$ is close to 0°, i.e. transition dipoles are almost orthogonal to the surface, $\left\langle ZXXZ \right\rangle_S$ is much larger in amplitude than $\left\langle XXXX \right\rangle_S$ because $\left| \mu \cdot \hat{\varepsilon}_{X_S} \right| \ll \left| \mu \cdot \hat{\varepsilon}_{Z_S} \right|$. On the other hand, in case $\left\langle \theta_S \right\rangle$ is close to 90°, because $\left| \mu \cdot \hat{\varepsilon}_{X_S} \right| \gg \left| \mu \cdot \hat{\varepsilon}_{Z_S} \right|$, the amplitude of $\left\langle ZXXZ \right\rangle_S$ is much smaller than $\left\langle XXXX \right\rangle_S$. Thus the approximation given in Eqs.

(D.20), which neglects the contribution from $\langle ZXXZ \rangle_S$, introduces large error for the first case, but almost no error for the latter case. Thus the error is expected to have strong correlation with the order parameter $\langle S \rangle$. $\langle S \rangle$ is directly related to the average polar angle $\langle \theta_S \rangle$ through Eq. (II.27), and it can be obtained from time averaged linear dichroism measurements.

In a typical experiment with BOXCARS geometry (Figure 10A), Φ will be less than 10°. In Figure 10A, if Φ is 10°, the angle formed by beams B2 and B3 is 20°, which is large for most experiments. We will consider the errors introduced by the approximations for $\Phi = 15^\circ, 10^\circ, 5^\circ, 2.5^\circ$ in the context of the wobbling-in-a-cone model with various cone angles θ_C (10° - 60°) and tilt angles θ_{tilt} (0° ~ 90°). The samples tilt angle χ was set to 35°. Once Φ, θ_C and θ_{tilt} are specified, the response functions in Eqs.(D.16), (D.18) and (D.20) can be evaluated. Then the errors introduced by the approximation are calculated by

$$E_{C22}(t) = \left| \left\{ R^{\chi=0^\circ}_{XXXX,\text{approx}}(t) - R^{\chi=0^\circ}_{XXXX}(t) \right\} \Big/ R^{\chi=0^\circ}_{XXXX}(t) \right| \tag{D.22}$$

$$E_{C23}(t) = \left| \left\{ R^{\chi=35^\circ}_{XXXX}(t) - R^{\chi=0^\circ}_{XXXX}(t) \right\} \Big/ R^{\chi=0^\circ}_{XXXX}(t) \right| \tag{D.23}$$

Eq. (D.22) is the error introduced by the approximation Eq. (D.20), and Eq. (D.23) is the error introduced by Eq.(D.21). As seen in Eqs. (D.22) and (D.23), the errors are time-dependent. For each set of conditions, we have determined the errors as a function of time and will present the worst errors. For each set of θ_C and θ_{tilt}, the order parameter $\langle S \rangle$ was calculated. The errors from Eqs. (D.22) and (D.23) were plotted with respect to order parameter $\langle S \rangle$ and are shown in Figure S2.A for Eq. (D.22)) and Figure S2.B Eq. (D.23). Because a given order parameter can arise from a range of θ_C and θ_{tilt}, there is a vertical width for each order parameter. As seen in Figure S2.A and S2.B, over a wide range of order parameters, the errors are less than 2%.

However, the error becomes significant as the order parameter increases, and range of acceptable errors is greater for smaller crossing angle Φ. As the order parameter approaches 1, not even a small crossing angle is useful in suppressing the errors. For large order parameters the planar HDTG geometry (Figure 9B) should be used, or a pump-probe experiment (Figure 9A) can be performed. These experiments do not require the approximations that are necessary for the HDTG experiment with BOXCARS geometry (Figure 10A).

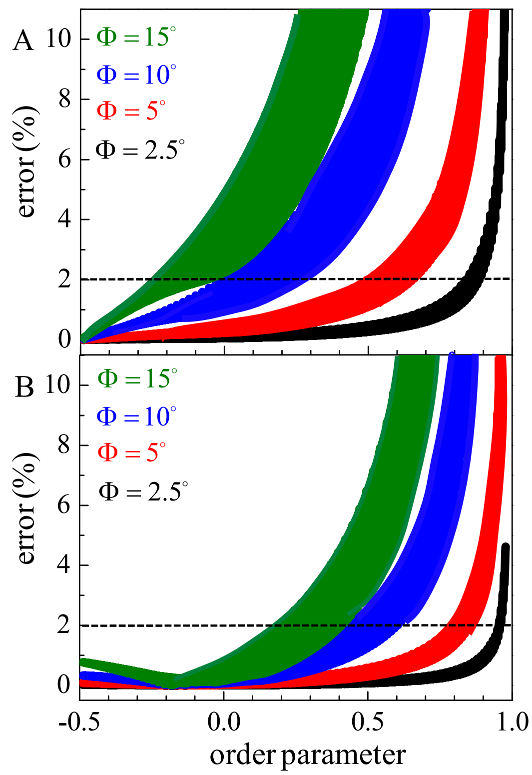

Figure S2. Errors introduced by the approximations with $\chi = 35°$ for $\Phi = 2.5°$ (black), $\Phi = 5°$ (red), $\Phi = 10°$ (blue), and $\Phi = 15°$ (green). For each set of Φ, the maximum error is shown as a function of the order parameter. A given order parameter is obtained from a range of θ_C and θ_{tilt}, which gives the vertical width for each crossing angle Φ. **A.** Approximation given in Eqs. (D.20) with the maximum error from Eqs. (D.22). **B.** Approximation given in Eqs. (D.21) with the maximum error from Eqs.(D.23).

3. Fluorescence geometry

As shown in Figure 10B, we assume that the excitation beam propagates along Z_L axis, and measurements are made with X_L and Y_L *E*-field polarizations. The emitted fluorescence is collected by a lens, so there is a cone of angles collected with the cone half-angle determined by the size and focal length of the lens. The emitted beam is collimated by the lens and passed through a polarizer to selectively detect the X_L polarization. A fluorescence photon is emitted from the sample with polar angle θ and azimuthal angle ϕ (Figure S3). The detected polarization for this photon, X_B (beam frame), is perpendicular to *k*-vector of the photon and also to the Y_L axis in lab frame. Because unit *k*-vector for this photon is given in lab frame by

$$\hat{k} = \sin\theta\cos\phi\cdot\hat{\varepsilon}_{X_L} + \sin\theta\sin\phi\cdot\hat{\varepsilon}_{Y_L} + \cos\theta\cdot\hat{\varepsilon}_{Z_L} \quad \text{(D.24)}$$

the X_B polarized *E*-field, $\hat{\varepsilon}_{X_B}$, can be expressed in the lab frame as

$$\hat{\varepsilon}_{X_B} = \frac{1}{\sqrt{\cos^2\theta + \sin^2\theta\cos^2\phi}}\left(\cos\theta\cdot\hat{\varepsilon}_{X_L} - \sin\theta\cos\phi\cdot\hat{\varepsilon}_{Z_L}\right) \quad \text{(D.25)}$$

Note that $\hat{\varepsilon}_{X_B}\cdot\hat{\varepsilon}_{Y_L} = 0$ and $\hat{\varepsilon}_{X_B}\cdot\hat{k} = 0$.

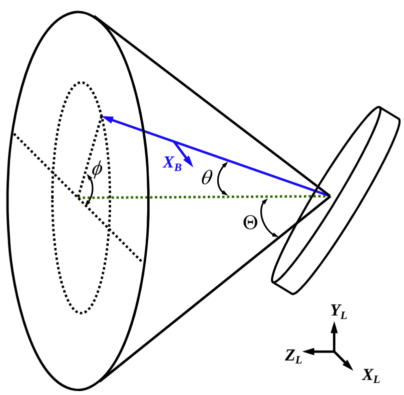

Figure S3. A cone of fluorescence is emitted following excitation by the pump beam. The direction of each photon is specified by the angles (θ,ϕ) shown in the figure. The emitted fluorescence is collected for θ = 0 to Θ and ϕ = 0 to 2π.

First consider the simplest case in which the polarization for the excitation beam is X_L and the sample is installed so that the surface is normal to the excitation beam ($\chi = 0^\circ$). In this case, $\hat{\varepsilon}_{X_S} = \hat{\varepsilon}_{X_L}$ and $\hat{\varepsilon}_{Y_S} = \hat{\varepsilon}_{Y_L}$ as in Eqs. (II.6) and (II.7). Thus for a specific photon emitted in the (θ,ϕ) direction, the response function is given by

$$\begin{aligned} R^{\chi=0^\circ}_{XXXX}(\theta,\phi) &= \Bigg\langle \left\{ \frac{\cos\theta}{\sqrt{\cos^2\theta+\sin^2\theta\cos^2\phi}} X - \frac{\sin\theta\cos\phi}{\sqrt{\cos^2\theta+\sin^2\theta\cos^2\phi}} Z \right\} \\ &\quad \left\{ \frac{\cos\theta}{\sqrt{\cos^2\theta+\sin^2\theta\cos^2\phi}} X - \frac{\sin\theta\cos\phi}{\sqrt{\cos^2\theta+\sin^2\theta\cos^2\phi}} Z \right\} XX \Bigg\rangle_S \\ &= \frac{\cos^2\theta}{\cos^2\theta+\sin^2\theta\cos^2\phi} \langle XXXX \rangle_S + \frac{\sin^2\theta\cos^2\phi}{\cos^2\theta+\sin^2\theta\cos^2\phi} \langle ZZXX \rangle_S \end{aligned} \tag{D.26}$$

The photons collected by the lens (see Figure 10B) are emitted in all directions within the collection cone, i.e. $\theta = 0$ to Θ and $\phi = 0$ to 2π. Thus the actual response function is given by

$$\begin{aligned} R^{\chi=0^\circ}_{XXXX} = \frac{1}{2\pi(1-\cos\Theta)} \Bigg[& \int_{\theta=0}^{\theta=\Theta} d\theta \sin\theta \int_{\phi=0}^{\phi=2\pi} d\phi \frac{\cos^2\theta}{\cos^2\theta+\sin^2\theta\cos^2\phi} \langle XXXX \rangle_S \\ & + \int_{\theta=0}^{\theta=\Theta} d\theta \sin\theta \int_{\phi=0}^{\phi=2\pi} d\phi \frac{\sin^2\theta\cos^2\phi}{\cos^2\theta+\sin^2\theta\cos^2\phi} \langle ZZXX \rangle_S \Bigg] \end{aligned} \tag{D.27}$$

which can be expressed using the spherical harmonics representations given in Table S.I to yield Eq. (V.10) in the main text. The response functions for the other sets of polarizations can be derived in the same way.

As pointed out in the main text, the fluorescence geometry has the same issue as the HDTG experiment with BOXCARS geometry in terms of scaling amplitudes between different configurations because the amplitudes of $R^{\chi=0^\circ}_{XXXX}$ and R^{χ}_{XXXX} will not be the same. The maximum error in the scaling was estimated for transition dipoles wobbling-in-a-cone, and is given by

$$E_{flscale} = \left| \left\{ R^{\chi=35^\circ}_{XXXX}(t) - R^{\chi=0^\circ}_{XXXX}(t) \right\} \Big/ R^{\chi=0^\circ}_{XXXX}(t) \right|, \tag{D.28}$$

where the subscript, *flscale*, stands for fluorescence scaling. The error calculations were done for various collection cone half angles $\Theta = 15°, 10°, 5°,$ and $2.5°$, and a range of cone angles θ_C (10° to 60°) and cone tilt angles θ_{tilt} (0° to 90°). The samples tilt angle χ was set to 35°. The results are shown in Figure S4. As shown in Figure S4, even a relatively large collection cone half angle of 15° works for a wide range of order parameter (−0.5 to ~0.5). For samples with an order parameter >0.5, Θ must be selected so that the difference between $R_{XXXX}^{\chi=0°}$ and R_{XXXX}^{χ} is small. $\Theta = 2.5°$ works for essentially any order parameter. It should be noted that the fluorescence geometry does not suffer from the emergence of $\left\langle Y_2^{1*} Y_2^1 \right\rangle$ in the response functions because the excitation beam is a single beam and the *X*-polarization is always set parallel to the X_S axis of the surface frame.

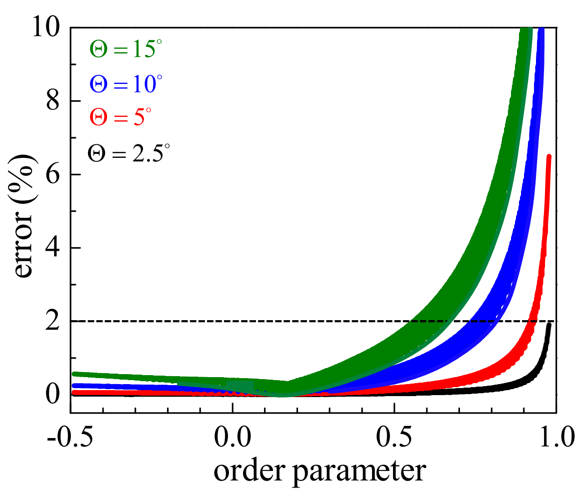

Figure S4. The scaling error introduced by the approximation (Eq. (D.28)) with $\chi = 35°$ for each fluorescence collection cone half angle Θ. $\Theta = 2.5°$ (black), $\Theta = 5°$ (red), $\Theta = 10°$ (blue), and $\Theta = 15°$ (green). For each Θ, the maximum error is shown as a function of the order parameter. A given order parameter is obtained from a range of θ_C and θ_{tilt}, which gives the vertical width to each plot for each cone half angle Θ.

References

1. C. C. Wang and R. Pecora, J. Chem. Phys. **72**, 5333-5340 (1980).
2. Z. Gengeliczki, D. E. Rosenfeld, and M. D. Fayer, J. Chem. Phys. **132**, 244703-244703 (2010).
3. A. Tokmakoff and M. D. Fayer, J. Chem. Phys. **103**, 2810-2826 (1995).
4. R. N. Zare, *Angular Momentum : Understanding Spatial Aspects in Chemistry and Physics*. (Wiley, New York, 1988).

TABLE S.1. Spherical harmonics representation (in the surface frame) of the integrals $\langle\delta\gamma\beta\alpha\rangle_S$ defined in Eq. (C.4).

$\langle\delta\gamma\beta\alpha\rangle_S$ integral	Spherical Harmonics Representation
$\langle XXXX\rangle_S, \langle YYYY\rangle_S$	$\frac{1}{9}-\frac{4}{9}\sqrt{\frac{\pi}{5}}\langle Y_2^0\rangle+\frac{4\pi}{45}\langle Y_2^{0*}Y_2^0\rangle+\frac{4\pi}{15}\langle Y_2^{2*}Y_2^2\rangle$
$\langle ZZZZ\rangle_S$	$\frac{1}{9}+\frac{8}{9}\sqrt{\frac{\pi}{5}}\langle Y_2^0\rangle+\frac{16\pi}{45}\langle Y_2^{0*}Y_2^0\rangle$
$\langle XXYY\rangle_S, \langle YYXX\rangle_S$	$\frac{1}{9}-\frac{4}{9}\sqrt{\frac{\pi}{5}}\langle Y_2^0\rangle+\frac{4\pi}{45}\langle Y_2^{0*}Y_2^0\rangle-\frac{4\pi}{15}\langle Y_2^{2*}Y_2^2\rangle$
$\langle XXZZ\rangle_S, \langle ZZXX\rangle_S, \langle YYZZ\rangle_S, \langle ZZYY\rangle_S$	$\frac{1}{9}+\frac{2}{9}\sqrt{\frac{\pi}{5}}\langle Y_2^0\rangle-\frac{8\pi}{45}\langle Y_2^{0*}Y_2^0\rangle$
$\langle XYXY\rangle_S, \langle YXXY\rangle_S, \langle XYYX\rangle_S, \langle YXYX\rangle_S$	$\frac{4\pi}{15}\langle Y_2^{2*}Y_2^2\rangle$
$\langle XZXZ\rangle_S, \langle ZXXZ\rangle_S, \langle XZZX\rangle_S, \langle ZXZX\rangle_S$, $\langle YZYZ\rangle_S, \langle ZYYZ\rangle_S, \langle YZZY\rangle_S, \langle ZYZY\rangle_S$	$\frac{4\pi}{15}\langle Y_2^{1*}Y_2^1\rangle$
Others	0